Excited-state absorption in thulium-doped materials in the near-infrared

Lauren Guillemot, Pavel Loiko, Jean-Louis Doualan, Alain Braud, Patrice Camy

To be published in Optics Express:

Title:	Excited-state absorption in thulium-doped materials in the near-infrared
Authors:	Lauren Guillemot,Pavel Loiko,Jean-Louis DOUALAN,Alain BRAUD,Patrice Camy
Accepted:	23 June 22
Posted	29 June 22
DOI:	https://doi.org/10.1364/OE.460176

Excited-state absorption in thulium-doped materials in the near-infrared

Lauren Guillemot,[1] Pavel Loiko,[1] Jean-Louis Doualan,[1] Alain Braud,[1] and Patrice Camy[1,*]

[1]Centre de Recherche sur les Ions, les Matériaux et la Photonique (CIMAP), UMR 6252 CEA-CNRS-ENSICAEN, Université de Caen Normandie, 6 Boulevard Maréchal Juin, 14050 Caen Cedex 4, France
**patrice.camy@ensicaen.fr*

Abstract: Excited-state absorption (ESA) is a key process for upconversion pumping schemes of thulium (Tm^{3+}) doped laser materials. We have systematically studied two ESA transitions in the near-infrared spectral range, namely $^3F_4 \rightarrow {}^3F_{2,3}$ (at ~1 µm) and $^3F_4 \rightarrow {}^3H_4$ (at ~1.5 µm), in various Tm^{3+}-doped fluoride (ZBLAN glass, cubic KY_3F_{10} and CaF_2, tetragonal $LiYF_4$ and $LiLuF_4$, monoclinic BaY_2F_8 crystals) and oxide (cubic $Y_3Al_5O_{12}$, orthorhombic $YAlO_3$ crystals) laser materials, using a pump-probe method with polarized light. An approach to calculate the constants of energy-transfer upconversion (ETU) is also presented.

1. Introduction

Excited-state absorption (ESA) is a process of excitation of a single atom, ion or molecule from a lower-lying excited-state |1> to a higher-lying one |2> with the absorption of a photon [1]. ESA can occur only if the system has been already excited to the |1> state from the ground-state |0> by ground-state absorption (GSA), Fig. 1. Therefore, the excitation to the |2> state via ESA involves at least two pump photons. The energy differences between the (|0> and |1>) and (|1> and |2>) states can be either similar (resonant) or different. In the latter case, two pump beams with different wavelengths are required to observe ESA. ESA is commonly observed in molecules and materials doped with transition metal (TM) ions [2-4]. It is less common for rare-earth (RE^{3+}) doped materials because of their narrow bandwidth transitions. Among RE^{3+} ions, a larger variety of ESA processes occurs for those exhibiting rich (ladder-like) energy-level schemes [5-7].

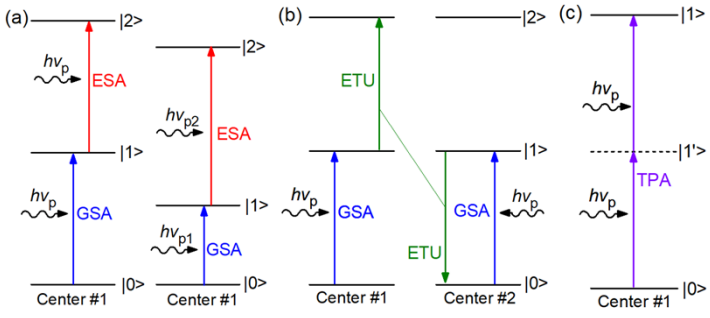

Fig. 1. Two-photon processes: (a) excited-state absorption, (b) energy-transfer upconversion and (c) two-photon absorption. |0>, ground-state, |1> and |2>, excited-states, |1'>, virtual state.

ESA should be distinguished from other two-ion or two-photon processes, such as energy-transfer upconversion (ETU) and two-photon absorption (TPA). For ETU, two neighboring centers are both excited to the |1> state and transfer non-radiatively the excitation energy, so that one ion is further excited to the higher-lying |2> state and another one returns to the ground-state |0> [8], Fig. 1. The probability of ETU depends on the concentration of centers and their spatial distribution [9,10]. TPA is a process of simultaneous absorption of two pump photons

with the same frequency leading to the population of an excited state |1> through a virtual state |1'>, Fig. 1. It is a third-order process, and its probability depends quadratically on the light intensity.

Frequently, ESA is used to obtain emission from higher-lying excited-states with a frequency ν_e being higher than the pump photon frequency ν_p (an anti-Stokes process). ESA can also assist in obtaining Stokes emissions from such higher lying states. In this way, ESA can be a key process for upconversion pumping of RE^{3+}-doped laser materials resulting in lasing in the infrared [11,12] or visible [13,14] spectral ranges. Concerning the latter, upconversion pumping is known for several rare-earth ions, such as Er^{3+}, Pr^{3+}, Tm^{3+} [15].

If the transitions |0> → |1> and |1> → |2> are not resonant in energy, the higher-lying excited-state can be populated either by using two different pump beams with photon frequencies ν_{p1} and ν_{p2}, or via the photon avalanche (PA) effect [16]. PA was first evidenced by Chivian *et al*. for Pr^{3+} ions [17]. Furthermore, it was used to demonstrate upconversion pumping of laser materials doped with Pr^{3+} [18], Nd^{3+} [19] and Tm^{3+} [20] ions. The typical scheme of PA is illustrated in Fig. 2. The first step is a non-resonant (phonon-assisted) GSA to the |1> state followed by a resonant ESA, |1> → |2>. The second step relies on the cross-relaxation (CR) process between two adjacent ions, one being in the higher-lying excited-state |2> and one - in the ground-state |0>. Because of the non-radiative energy transfer, the first one experiences a de-excitation to the intermediate state |1> and the second one is promoted to the same state. As a consequence, the population of the |1> state increases thus feeding the ESA process. In this way, the higher lying |2> state is efficiently populated even if the first GSA transition is non-resonant.

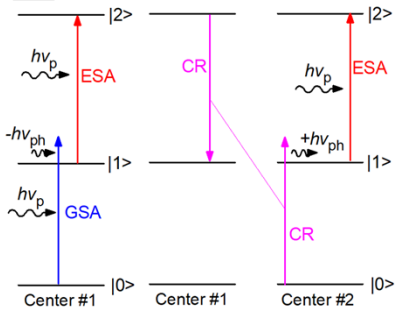

Fig. 2. Photon avalanche effect scheme: GSA and ESA – ground- and excited-state absorption, respectively, CR – cross-relaxation, $-h\nu_{ph}$ and $+h\nu_{ph}$ – absorption / generation of phonons.

Among the rare-earth ions, thulium (Tm^{3+}) is attracting a lot of attention for coherent light generation in the short-wavelength-infrared (SWIR) spectral range. Tm^{3+} has an electronic configuration of $[Xe]4f^{12}$ and its simplified scheme of energy levels is shown in Fig. 3(a). The most widely exploited Tm^{3+} laser transition originates from the metastable $^3F_4$ state ($^3F_4 \rightarrow {}^3H_6$, at ~2 μm) [21] and less common ones – from the higher-lying $^3H_4$ state ($^3H_4 \rightarrow {}^3F_4$, at ~1.5 μm and $^3H_4 \rightarrow {}^3H_5$, at ~2.3 μm [22]).

To achieve laser emission in all these channels, Tm^{3+} ions are typically excited to the $^3H_4$ state owing to the intense $^3H_6 \rightarrow {}^3H_4$ GSA transition spectrally overlapping with the emission of commercial AlGaAs laser diodes and Ti:Sapphire lasers. The CR process, $^3H_4 + {}^3H_6 \rightarrow {}^3F_4 + {}^3F_4$, Fig. 3(b), is very efficient in many Tm^{3+}-doped materials even at moderate doping levels, resulting in efficient population of the $^3F_4$ metastable state with a pump quantum efficiency approaching 2 (a two-for-one pump process) [23] and giving rise to high laser efficiencies particularly at ~2 μm well exceeding the Stokes limit [24].

Owing to the complex ladder-like structure of Tm^{3+} energy levels, the presence of efficient CR process and a long-living metastable level, the upconversion pumping of Tm^{3+}-doped materials relying on the PA effect for lasing at ~2.3 μm was also realized recently [20,25], Fig. 3(c). It is based on the non-resonant GSA $^3H_6 \rightarrow {}^3H_5$ followed by multiphonon NR

relaxation to the metastable level $^3F_4$, followed by a resonant ESA $^3F_4 \rightarrow {}^3F_{2,3}$ and efficient CR. Altogether, this leads to efficient population of both the $^3F_4$ and $^3H_4$ states.

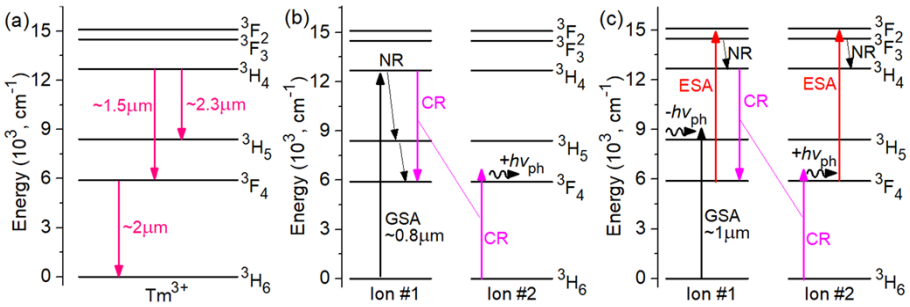

Fig. 3. Thulium ions: (a) simplified energy-level scheme showing laser transitions in the near- and mid-infrared; (b-c) pumping schemes of Tm^{3+} ions: (b) conventional pumping; (c) upconversion pumping, GSA and ESA – ground- and excited-state absorption, CR - cross-relaxation, NR – multiphonon non-radiative relaxation.

As explained above, excited-state absorption is a key effect for realization of upconversion pumping of Tm lasers emitting in the mid-infrared, at ~2.3 μm. Such lasers find applications in sensing of atmospheric species such as HF, CO, CH_4 or H_2CO, non-invasive glucose ($C_6H_{12}O_6$) blood measurements, or frequency conversion further in the mid-infrared. Unfortunately, to date, the information about the near-infrared ESA properties of commonly used Tm^{3+}-doped laser crystals is relatively scarce.

In the present work, we aimed to perform a systematic study of excited-state absorption of Tm^{3+} ions in the near-infrared for a series of laser host materials (fluorides and oxides).

2. Methodology

2.1 Excited-state absorption by thulium ions

Figure 4 summarized the excited-state absorption transitions of Tm^{3+} ions exploited so far. The corresponding ground-state absorption transitions are shown as well. Note that we consider the case of resonant energy differences between the (|0> and |1>) and (|1> and |2>) states, Fig. 1(a). The transition $^3F_4 \rightarrow {}^1D_2$ falls in the blue spectral range (~0.45 μm) and is resonant with the $^3H_6 \rightarrow {}^1G_4$ GSA channel. The transitions $^3H_4 \rightarrow {}^1D_2$ and $^3F_4 \rightarrow {}^1G_4$ both in the red are nearly resonant with the $^3H_6 \rightarrow {}^3F_{2,3}$ GSA channel; they are crucial for demonstrating upconversion pumping of blue thulium lasers [26-28]. The ESA properties of various Tm^{3+} doped materials in the red spectral range have been extensively studied in the past [5,29].

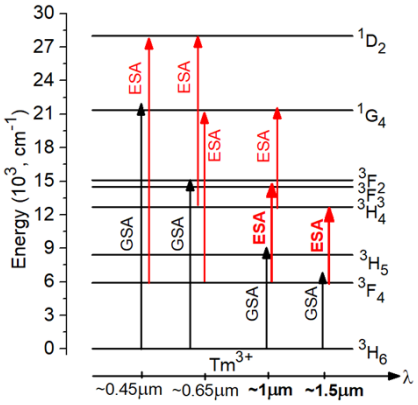

Fig. 4. Summary of excited-state absorption transitions of thulium ions exploited so far (*bold arrows* – this work), the corresponding ground-state absorption is also shown.

In the near-IR, the ESA transitions $^3F_4 \rightarrow {}^3F_{2,3}$ and $^3H_4 \rightarrow {}^1G_4$ at ~1 μm are close in energy with the $^3H_6 \rightarrow {}^3H_5$ GSA channel. The $^3F_4 \rightarrow {}^3H_4$ ESA transition at ~1.5 μm is close to the $^3H_6 \rightarrow {}^3H_5$ GSA channel. In the present work, we focus on two near-infrared ESA transitions, $^3F_4 \rightarrow {}^3F_{2,3}$ and $^3F_4 \rightarrow {}^3H_4$, which are relevant for UC pumping of mid-infrared Tm lasers. So far, these ESA channels have been studied only for Tm:$Y_3Al_5O_{12}$ [30]. Some incomplete ESA data were also reported for Tm:KY_3F_{10} and Tm:$LiYF_4$ [31].

2.2 Experimental setup

The measurements of the ESA spectra of Tm^{3+}-doped materials corresponding to the $^3F_4 \rightarrow {}^3F_{2,3}$ and $^3F_4 \rightarrow {}^3H_4$ transitions were carried out using a pump-probe method [1,32]. Its principle is the following: the first intense laser beam (the pump) excites Tm^{3+} ions into the metastable $^3F_4$ state. The second weak beam (the probe) propagates through the pumped area of the sample revealing the additional absorption caused by ESA.

The scheme of the pump-probe set-up is shown in Fig. 5. The sample was prepared as a relatively thin (a few mm thick) plane-parallel plate with both faces polished to laser quality to avoid scattering of the pump. It was placed between two pinholes (diameter: 500 μm) placed close to the sample faces. This provided a good spatial overlap between the pump and the probe beams, as well as helped to limit the spot size of the probe in the sample.

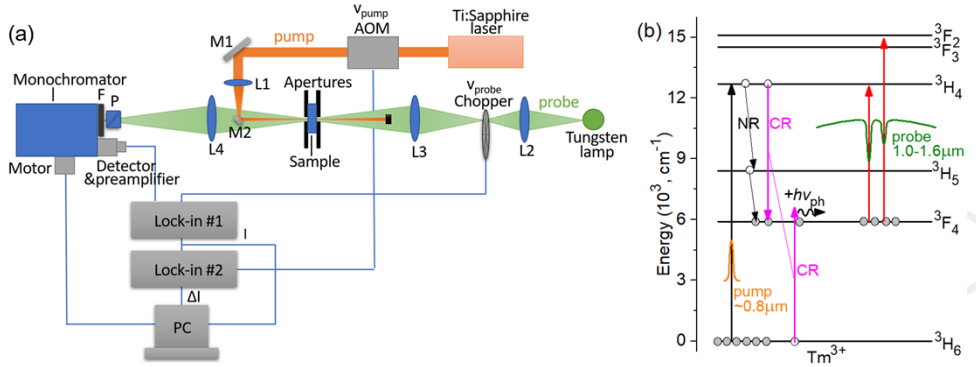

Fig. 5. (a) Scheme of the pump-probe setup used for ESA measurements: AOM, acousto-optic modulator, M1 and M2, folding mirrors, L1, focusing lens, L2 – L4, wide-aperture lenses, ν_{pump} and ν_{probe}, pump and probe modulation frequencies, respectively, P, polarizer, F, filter; (b) Energy-level scheme of Tm^{3+} ions illustrating the principle of the pump-probe method.

As a source of pump radiation, we used a continuous-wave Ti:Sapphire laser (Coherent 890) delivering up to 1.5 W at ~0.8 μm in the fundamental transverse mode ($M^2 \approx 1$). The pump wavelength was tuned to match precisely the maximum of the $^3H_6 \rightarrow {}^3H_4$ Tm^{3+} absorption band of the studied material. The pump beam was modulated at low frequency ($\nu_{pump} \approx 10$ Hz) by an acousto-optic modulator (Isomet, model 1205C-2) and it was focused into the sample using a lens L1 (f = 150 mm) resulting in a spot size (diameter) of ~300 μm. The single-pass pump absorption was >50%. This resulted in a relatively uniform distribution of inversion through the sample.

A 100 W halogen-tungsten white-light lamp (Oriel, model 66184) with a broad emission spectrum close to that of a black body was used as a probe source. Its output was modulated at a higher frequency ($\nu_{probe} \approx 1$ kHz) by a mechanical chopper. The probe beam was also focused into the sample using a pair of wide-aperture lenses L2 and L3 (f = 50 mm and 100 mm, respectively) and after passing the sample, it was reimaged on the input slit of the monochromator using the lens L4 (f = 100 mm).

For measuring the spectra, a 0.64 m monochromator (Jobin-Yvon, HRS2) and an InGaAs detector with two lock-in amplifiers (SR810 DSP, Stanford Research Systems) were used. The first one was locked with the pump modulation frequency ν_{pump} and measured the average

intensity transmitted through the sample I and the second one was locked with the probe frequency ν_{probe} to measure the pump-induced variation ΔI of the abovementioned transmission. For the developed setup, the transmission variation $\Delta I/I$ was about ~10^{-4}...10^{-3} at the wavelengths of the ESA peaks.

A Glan-Taylor polarizer was placed before the input slit of the monochromator for polarization-resolved measurements. A long-pass filter (LP950, Spectrogon) was also used to filter out the residual pump radiation.

The wavelength calibration was performed with a mercury vapor lamp (Schwabe, Sp 60/U-V). The measurements were performed in the spectral range of 950-1575 nm with a resolution (spectral bandwidth, SBW) of 1-2 nm, depending on the sample. All the studies were performed at room temperature (RT, 20 °C).

2.3 Materials

Table 1 presents the list of the Tm^{3+}-doped fluoride (ZBLAN glass, KY_3F_{10}, CaF_2, $LiYF_4$, $LiLuF_4$ and BaY_2F_8 crystals) and oxide ($Y_3Al_5O_{12}$ and $YAlO_3$ crystals) laser materials that have been studied.

To ensure that no ESA from the $^3H_4$ pump level (e.g., the $^3H_4 \rightarrow {}^1G_4$ transition at ~1 μm, cf. Fig. 4) can contribute to the measured spectra, we used highly Tm^{3+}-doped materials (several at.% Tm, Table 1) providing efficient self-quenching of the $^3H_4$ lifetime by cross-relaxation. Under these conditions, a favorable ratio of the $^3F_4$ to $^3H_4$ lifetimes ($\tau_{lum}(^3F_4)$ of about few ms and $\tau_{lum}(^3F_4)$ of about few tens of μs) was observed.

Table 1. Summary of the Studied Thulium-Doped Materials

Glass / crystal	Tm doping	Crystal class (sp.gr.)	Optical property	Tm^{3+} site
ZBLAN glass	1.0 wt%	amorphous	isotropic	-
KY_3F_{10}	5.0 at.%	cubic (*Fm*$\bar{3}$*m*)	isotropic	C_{4v} (Y^{3+})
CaF_2	1.5 at.%	cubic (*Fm*$\bar{3}$*m*)	isotropic	clusters
$LiYF_4$	3.0 at.%	tetragonal ($I4_1/a$)	uniaxial (+)	S_4 (Y^{3+})
$LiLuF_4$	9.3 at.%	tetragonal ($I4_1/a$)	uniaxial (+)	S_4 (Lu^{3+})
BaY_2F_8	0.5 at.%	monoclinic (*C*2/*m*)	biaxial	C_2 (Y^{3+})
$Y_3Al_5O_{12}$	3.2 at.%	cubic (*Ia*$\bar{3}$*d*)	isotropic	D_2 (Y^{3+})
$YAlO_3$	1.5 at.%	orthorhombic (*Pnma*)	biaxial	C_s (Y^{3+})

For the optically isotropic glass and cubic crystals (KY_3F_{10}, CaF_2 and $Y_3Al_5O_{12}$), the studies were performed using unpolarized light. For the optically uniaxial crystals ($LiYF_4$ and $LiLuF_4$, the optical axis is parallel to the ***c***-axis), the measurements were performed using ***a***-cut samples for the two principal light polarizations, π (***E*** || ***c***) and σ (***E*** ⊥ ***c***). For the optically biaxial crystals (BaY_2F_8 and $YAlO_3$), several samples with different cuts were used giving access to three principal light polarizations. For monoclinic BaY_2F_8, they were denoted as ***E*** || X, Y and Z (X, Y and Z are the optical indicatrix axes; their assignment is given in [33]). For orthorhombic $YAlO_3$, the optical indicatrix frame coincides with the crystallographic one, so that the polarizations were denoted simply as ***E*** || ***a***, ***b*** and ***c***. Here, the crystallographic axes are selected according to the standard crystallographic setting *Pnma* [34].

2.4 Methodology

The relative variation of the transmitted probe signal $\Delta I/I$ is given by [32]:

$$\frac{\Delta I}{I}(\lambda) = AN^{*}L(\sigma_{GSA}(\lambda) + \sigma_{SE}(\lambda) - \sigma_{ESA}(\lambda)), \quad (1)$$

where A is a calibration factor, L is the optical length of the sample, N^* is the population of the probed excited-state, the $^3F_4$ state of Tm^{3+}, in our case (these three parameters are independent of the wavelength and they are determined by the geometry of the pump-probe experiment), σ_{GSA} and σ_{ESA} are the ground- and excited-state absorption cross-sections, respectively, σ_{SE} is the stimulated-emission (SE) cross-section. The σ_{GSA} and σ_{SE} values are found independently

and the corresponding spectral bands can be used for calibrating the set-up (i.e., determining the constant value of AN^*L for each particular sample). In this way, the spatial and longitudinal distributions of the population of the metastable excited-state |1> do not affect the measured ESA spectra. Equation (1) represents the first-order development of the transmission of the probe light and its is valid in the case of relatively weak $\Delta I/I$ variations [32].

There are two Tm^{3+} emissions falling in the studied spectral range, namely $^3H_4 \rightarrow {}^3F_4$ (at ~1.5 μm) and $^3F_4 \rightarrow {}^3H_6$ (at ~2 μm). The former emission originates from the $^3H_4$ state which is different from the probed one ($^3F_4$). The spectral overlap of the ESA spectra extending from ~1 to 1.6 μm with the second emission is very weak. Thus, for simplicity, we assume $\sigma_{SE} \approx 0$ in Eq. 1.

For the $^3F_4 \rightarrow {}^3H_4$ transition (at ~1.5 μm), the ESA cross-sections can be independently calculated using the reciprocity method [35] from the σ_{SE} spectra of the $^3H_4 \rightarrow {}^3F_4$ transition:

$$\sigma_{ESA}(\lambda) = \sigma_{SE}(\lambda)\frac{Z_2}{Z_1}\exp\left[\frac{(hc/\lambda) - E_{ZPL}}{kT}\right], \quad (2)$$

where h the Planck constant, c is the speed of light, λ is the light wavelength (hc/λ is the photon energy), k is the Boltzmann constant, T the sample temperature (RT), E_{ZPL} is the energy of the zero-phonon-line (ZPL) transition between the lowest Stark sub-levels of both multiplets, and $Z_{1(2)}$ are the partition functions of the lower and upper multiplets, respectively:

$$Z_m = \sum_k g_k^m e^{-\frac{E_k^m}{kT}}, \quad (3)$$

where each Stark sub-level has a number k, an energy E^m_k measured from the lowest sub-level of each multiplet and a degeneracy g^m_k.

The ESA spectra for the $^3F_4 \rightarrow {}^3F_{2,3}$ transition cannot be calculated by the reciprocity method because the $^3F_{2,3}$ states are depopulated by efficient multiphonon NR relaxation (the energy-gap to the lower-lying $^3H_4$ state is ~1800 cm^{-1}) and does not exhibit detectable luminescence.

2.5 Methodology: The case study of $Tm:LiYF_4$

To illustrate the analysis procedure of measuring and interpreting the Tm^{3+} ESA spectra, we have selected the $Tm:LiYF_4$ crystal. So far, it is the most widely used material for laser operation of Tm^{3+} ions in the mid-infrared. Figure 6 shows the raw spectrum, $\sigma_{GSA} - \sigma_{ESA}$, proportional to the $\Delta I/I$ ratio, the independently determined σ_{GSA} spectra for the $^3H_6 \rightarrow {}^3H_5$ and $^3H_6 \rightarrow {}^3F_4$ transitions (obtained from classical absorption studies) and the σ_{SE} spectra for the $^3H_4 \rightarrow {}^3H_5$ and $^3F_4 \rightarrow {}^3H_6$ transitions (obtained from emission spectra). The same figure shows the ESA spectra determined using Eq. (1). Following state-of-the-art studies [1], they are plotted in the range of negative cross-sections, i.e., as ($-\sigma_{ESA}$).

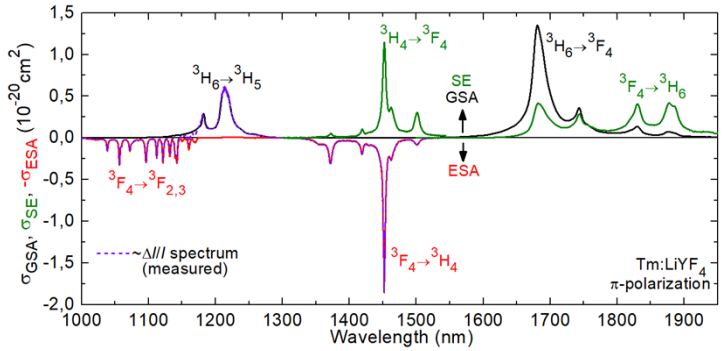

Fig. 6. Evaluation of the ESA cross-section spectra, σ_{ESA}, for the $Tm:LiYF_4$ crystal in the near-infrared: *violet* – calibrated raw spectrum ~$\Delta I/I$, *black* – σ_{GSA} spectra, *green* – σ_{SE} spectra, red - σ_{ESA} spectra. The light polarization is π.

Table 2. Crystal-Field Splitting of Selected Tm^{3+} Multiplets in $LiYF_4$

$^{2S+1}L_J$		E, cm^{-1}	Γ_i	$^{2S+1}L_J$		E, cm^{-1}	Γ_i	$^{2S+1}L_J$		E, cm^{-1}	Γ_i
$^3F_4$	Y_1	5599	1	$^3H_4$	W_1	12599	2	$^3F_3$	V_1	14520	3,4
	Y_2	5756	1		W_2	12624	1		V_2	14529	2
	Y_3	5757	3,4		W_3	12643	3,4		V_3	14594	3,4
	Y_4	5820	2		W_4	12745	1		V_4	15594	2
	Y_5	5942	2		W_5	12804	1		V_5	14597	1
	Y_6	5968	1		W_6	12835	3,4	$^3F_2$	U_1	15094	2
	Y_7	5972	3,4		W_7	12891	2		U_2	15203	3,4
									U_3	15232	2
									U_4	15275	1

To confirm our assignment of the measured ESA spectral bands, we have calculated the full set of wavelengths corresponding to electronic transitions between the Stark sub-levels of the involved Tm^{3+} multiplets ($^3F_4$ and $^3H_4$ + $^3F_{2,3}$). For this, the data on the crystal-field splitting for Tm^{3+} ions in $LiYF_4$ were used [36], Table 2. Here, we use empirical notations for Stark sub-levels ($^3F_4 = Y_i$, $^3H_4 = W_j$, $^3F_3 = V_k$, $^3F_2 = U_m$, where the subscripts i, j, etc., number the sub-levels starting from 1) proposed by Lupei *et al.* [37], as well as indicate the irreducible representations (Γ_1, Γ_2 or $\Gamma_{3,4}$) for each sub-level.

The polarization selection rules for electric-dipole (ED) and magnetic-dipole (MD) transitions for ions in S_4 sites are listed in Table 3. The MD transitions are those following the selection rules $\Delta J = |J - J'| = 0, \pm 1$, except of $0 \leftrightarrow 0'$. In our case, the ESA transitions $^3F_4 \rightarrow {}^3F_3$ and $^3F_4 \rightarrow {}^3H_4$ can have a MD contribution. Indeed, the Judd-Ofelt calculations for Tm^{3+} ions in $LiYF_4$ predict the following ED and MD probabilities of spontaneous radiative transitions: $A_{ED} = 51.35\ s^{-1}$ and $A_{MD} = 18.95\ s^{-1}$ (for $^3H_4 \rightarrow {}^3F_4$) and $A_{ED} = 44.09\ s^{-1}$ and $A_{MD} = 35.49\ s^{-1}$ (for $^3F_3 \rightarrow {}^3F_4$) [38]. Thus, the MD contribution to the ESA probabilities is expected to be non-negligible, especially for the $^3F_4 \rightarrow {}^3F_3$ transition. The extra MD lines should correspond to transitions between the Stark sub-levels having the same irreducible representations, i.e., $\Gamma_1 \rightarrow \Gamma_1$ and $\Gamma_2 \rightarrow \Gamma_2$, only for π-polarization, cf. Table 3.

Table 3. Polarization Selection Rules for Electric- and Magnetic-Dipole Transitions in S_4 Sites

ED	Γ_1	Γ_2	$\Gamma_{3,4}$	MD	Γ_1	Γ_2	$\Gamma_{3,4}$
Γ_1	...	π	σ	Γ_1	π	...	σ
Γ_2	π	...	σ	Γ_2	...	π	σ
$\Gamma_{3,4}$	σ	σ	π	$\Gamma_{3,4}$	σ	σ	π

The results on the assignment of the measured ESA spectra of Tm^{3+} ions to ED and MD allowed electronic transitions are shown in Fig. 7. Several conclusions can be drawn from this figure. First, the observed ESA lines are well assigned only to transitions originating from the $^3F_4$ state and terminating at the $^3H_4$ and $^3F_{2,3}$ ones (i.e., extra lines due to possible ESA from the $^3H_4$ state are not observed). Second, the polarization selection rules well explain the polarization anisotropy of ESA spectra. Third, the prominent ESA peaks can be in most cases assigned to single electronic transitions which determine their narrow-linewidth nature. Moreover, the ESA transitions terminating at the closely located $^3F_3$ and $^3F_2$ states are well resolved.

Figure 7(b,d) also contains the ESA cross-section spectra for the $^3F_4 \rightarrow {}^3H_4$ transition calculated by means of the reciprocity method. They are in good agreement with the measured ones confirming the correctness of the pump-probe-based approach.

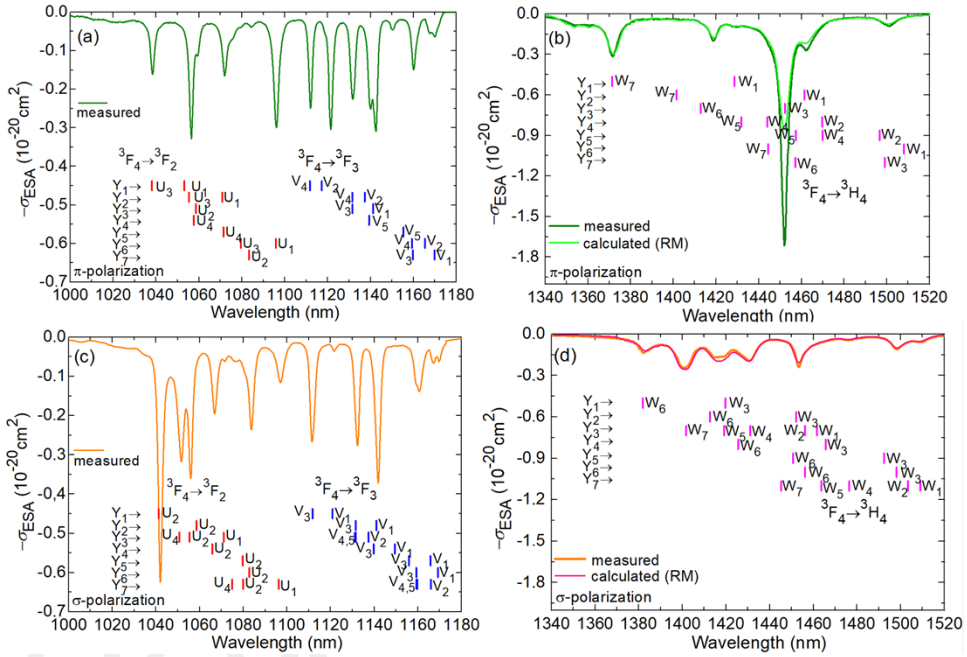

Fig. 7. Interpretation of the polarized ESA cross-section, σ_{ESA}, spectra for Tm^{3+} ions in the $LiYF_4$ crystal in the near-infrared: (a,c) the $^3F_4 \rightarrow {}^3F_{2,3}$ transitions, (b,d) the $^3F_4 \rightarrow {}^3H_4$ transition, light polarizations are (a,b) π and (c,d) σ. *Curves* – measured spectra, in (c,d), spectra calculated using the reciprocity method (RM) are shown for comparison, *vertical dashes* – ED electronic transitions of Tm^{3+} ions according to the polarization selection rules.

3. Excited-state absorption spectra

3.1 Fluoride materials

The ESA cross-section spectra corresponding to the $^3F_4 \rightarrow {}^3F_{2,3}$ and $^3F_4 \rightarrow {}^3H_4$ transitions for Tm^{3+} ions in fluoride materials (ZBLAN glass, cubic KY_3F_{10} and CaF_2, tetragonal $LiYF_4$ and $LiLuF_4$ and monoclinic BaY_2F_8 crystals) are shown in Fig. 8. Let us briefly discuss them.

Due to its amorphous nature, the Tm:ZBLAN glass shows smooth and broad bands at the expense of low peak ESA cross-sections. For the $^3F_4 \rightarrow {}^3F_{2,3}$ ESA transition which is of interest for UC pumping at ~1 μm, σ_{ESA} is 0.23×10^{-20} cm^2 at 1056 nm and the corresponding absorption bandwidth (full width at half maximum, FWHM) $\Delta\lambda_{ESA}$ is 39 nm. As Tm:ZBLAN glasses are used in the form of fibers, relatively high absorption via UC pumping is easily achievable. A ~2.3 μm Tm:ZBLAN fiber lasers with UC pumping at ~1 μm was recently reported [25].

Among the studied Tm^{3+}-doped fluoride crystals, Tm:CaF_2 is standing apart: its spectra are similar to those of the glass. Such a "glassy-like" behavior is due to the strong ion clustering even at low doping levels leading to significant inhomogeneous spectral broadening [39]. For the $^3F_4 \rightarrow {}^3F_{2,3}$ ESA transition, σ_{ESA} is low, only 0.07×10^{-20} cm^2 at 1064 nm with broad $\Delta\lambda_{ESA}$ of 38 nm. The origin of the ESA peak at 1089.7 nm is not clear; absorption of residual isolated Tm^{3+} ions in cubic symmetry sites (O_h) can explain this sharp line.

Other Tm^{3+}-doped fluoride crystals exhibit much narrower ESA peaks owing to electronic transitions of ions located in a single type of sites with reduced inhomogeneous broadening (cf. Table 1). For cubic Tm:KY_3F_{10}, σ_{ESA} reaches 0.91×10^{-20} cm^2 at 1067.7 nm with $\Delta\lambda_{ESA}$ = 3.4 nm. Another intense ESA line is observed at 1048.7 nm corresponding to a σ_{ESA} value of 0.73×10^{-20} cm^2 and a $\Delta\lambda_{ESA}$ of 3.6 nm. This line was recently used for demonstrating UC pumping of a ~2.3 μm Tm:KY_3F_{10} laser [40].

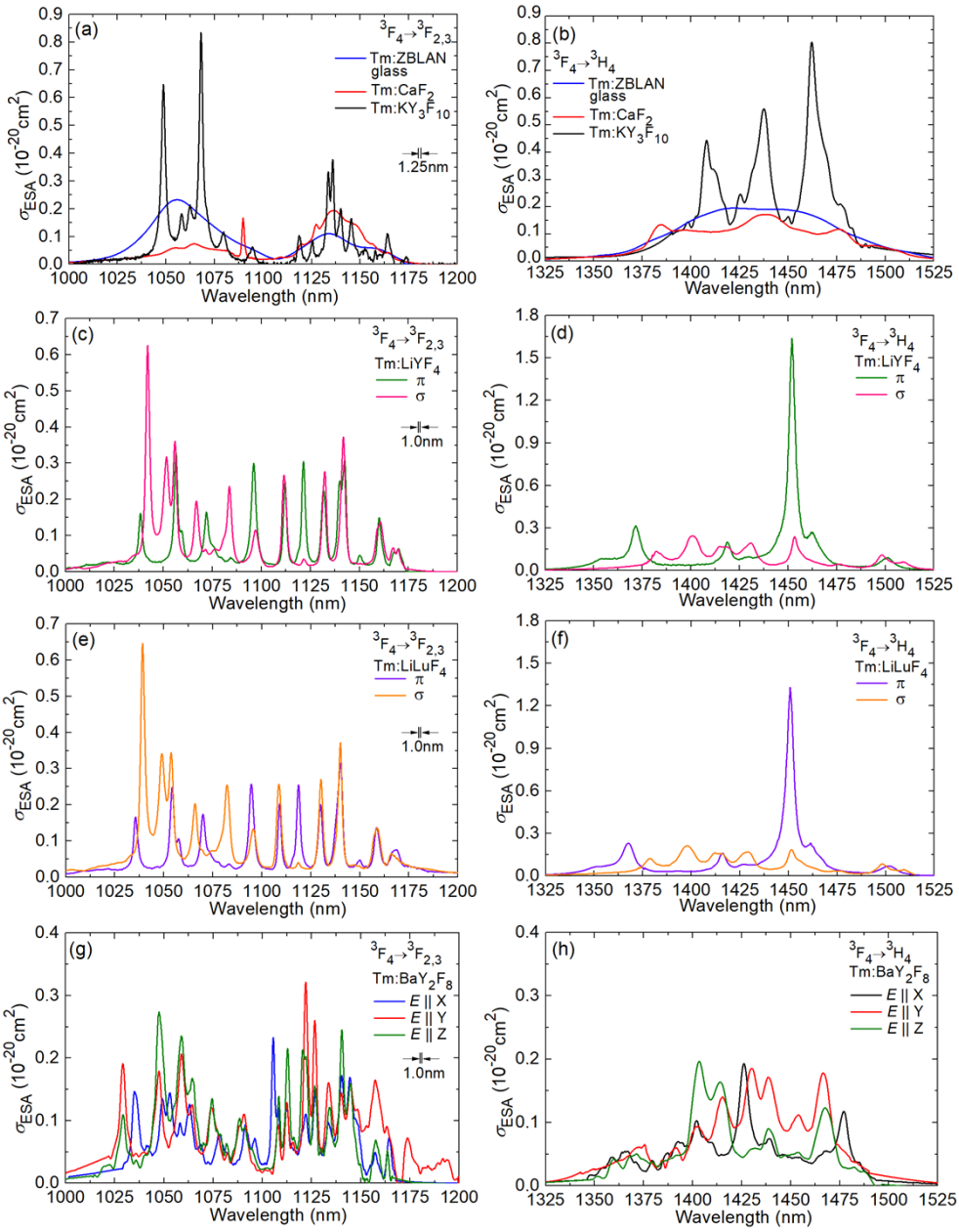

Fig. 8. Polarized (where applicable) ESA cross-section, σ_{ESA}, spectra for Tm^{3+} ions in fluoride materials: (a, b) isotropic hosts: ZBLAN glass, cubic KY_3F_{10} and CaF_2 crystals; (c-f) uniaxial crystals: (c,d) tetragonal $LiYF_4$ and (e,f) $LiLuF_4$ and (g,h) biaxial crystal: monoclinic BaY_2F_8. Transitions: (a,c,e,g) $^3F_4 \rightarrow {}^3F_{2,3}$ and (b,d,f,h) $^3F_4 \rightarrow {}^3H_4$. The spectral resolution is indicated on the graphs (it is the same in left and right panels).

For optically uniaxial and biaxial fluoride crystals, a noticeable polarization-anisotropy of ESA spectra is observed. For the $^3F_4 \rightarrow {}^3F_{2,3}$ ESA transition of Tm^{3+} ions in tetragonal $LiYF_4$ and $LiLuF_4$ crystals, higher ESA cross-sections are measured for σ-polarized light: σ_{ESA} reaches 0.62×10^{-20} cm^2 at 1042.0 nm and 0.36×10^{-20} cm^2 at 1055.9 nm with $\Delta\lambda_{ESA}$ = 2.5 nm and 3.2 nm, respectively (Tm:$LiYF_4$, σ-polarization). Both these ESA lines were used for UC pumping of a ~2.3 μm Tm:$LiYF_4$ laser [20]. The ESA properties of the isostructural LiY/LuF_4 crystals are

similar, while the ESA cross-sections seem to be slightly higher for the Lu-compound. Finally, for monoclinic Tm:BaY_2F_8, the preferable light polarization for UC pumping at ~1 μm is ***E*** || Z, as the corresponding σ_{ESA} reaches 0.27×10^{-20} cm^2 at 1047.2 nm with $\Delta\lambda_{ESA}$ = 5.5 nm.

Among the studied fluoride materials, Tm:KY_3F_{10} and Tm:LiY/LuF_4 crystals offer the most intense ESA lines around ~1 μm making them attractive for UC pumping.

3.2 Oxide materials

The ESA cross-section spectra corresponding to the $^3F_4 \rightarrow {}^3F_{2,3}$ and $^3F_4 \rightarrow {}^3H_4$ transitions for Tm^{3+} ions in oxide crystals (cubic $Y_3Al_5O_{12}$ and orthorhombic $YAlO_3$) are shown in Fig. 9.

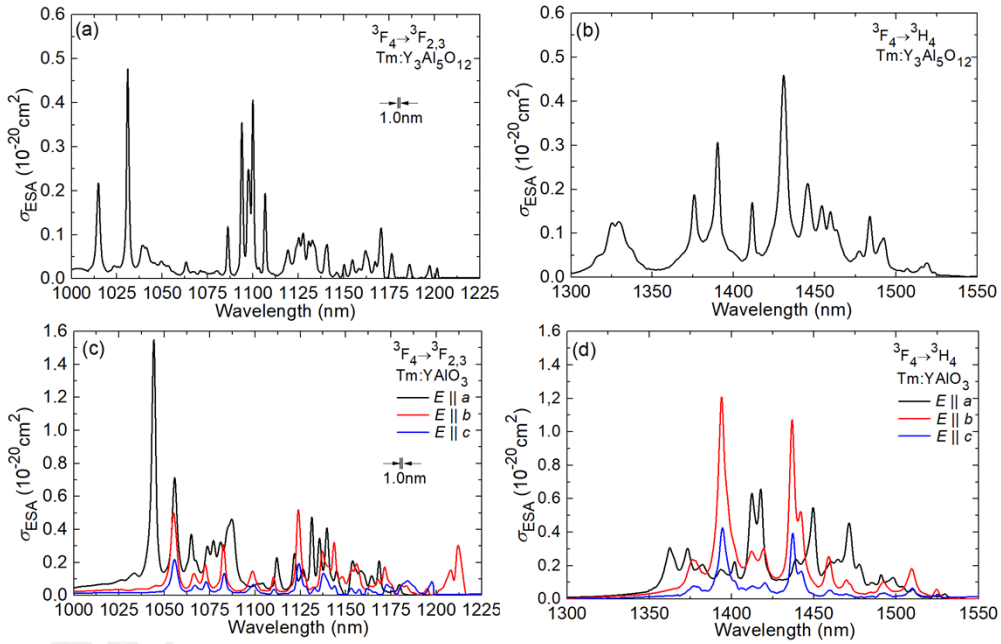

Fig. 9. Polarized (where applicable) ESA cross-section, σ_{ESA}, spectra for Tm^{3+} ions in oxide crystals: (a,b) cubic $Y_3Al_5O_{12}$ and (c,d) orthorhombic $YAlO_3$ crystals. Transitions: (a,c) $^3F_4 \rightarrow {}^3F_{2,3}$ and (b,d) $^3F_4 \rightarrow {}^3H_4$. The spectral resolution is indicated on the graphs.

For cubic Tm:$Y_3Al_5O_{12}$, the $^3F_4 \rightarrow {}^3F_{2,3}$ ESA transition, σ_{ESA} reaches 0.48×10^{-20} cm^2 at 1031.0 nm with a relatively narrow $\Delta\lambda_{ESA}$ of 1.5 nm.

For orthorhombic Tm:$YAlO_3$, the ESA spectra exhibit a significant polarization anisotropy. The most attractive polarization is ***E*** || ***a*** for which σ_{ESA} is 1.55×10^{-20} cm^2 (the highest value among the studied materials) at 1044.2 nm corresponding to $\Delta\lambda_{ESA}$ of 2.7 nm.

3.3 Towards upconversion pumping at ~1 μm

Table 4 lists the ESA peaks slightly above 1 μm (the $^3F_4 \rightarrow {}^3F_2$ transition) which are of practical interest for realization of upconversion pumping of ~2.3 μm Tm lasers. The corresponding pump sources can be commercially available Yb bulk or fiber lasers offering power-scalable output as well as wavelength tunability in this spectral range.

Table 4. Excited-State Absorption Peaks* of Tm^{3+} Ions in Fluoride and Oxide Materials Suitable for Upconversion Pumping at ~1 μm

Material	***E***	λ_{ESA}, nm	σ_{ESA}, 10^{-20} cm^2	$\Delta\lambda_{ESA}$, nm	Material	***E***	λ, nm	σ_{ESA}, 10^{-20} cm^2	$\Delta\lambda_{ESA}$, nm
ZBLAN	-	~1056	0.23	39	BaY_2F_8	***E*** ∥ X	1035.0	0.15	4.5
CaF_2	-	~1064	0.07	38			1049.2	0.13	9.4
KY_3F_{10}	-	1048.7	0.73	3.6			1053.0	0.14	4.9
		1057.9	0.20	5.0			1064.0	0.13	
		1062.1	0.27	5.0		***E*** ∥ Y	1029.2	0.19	4.7
		1067.7	0.91	3.4			1047.5	0.18	6.2
$LiYF_4$	π	1038.3	0.16	2.4			1058.9	0.21	9.5
		1056.5	0.32	2.2			1064.4	0.13	
	σ	1042.0	0.62	2.5		***E*** ∥ Z	1029.3	0.11	4.6
		1051.6	0.32	4.3			1047.5	0.27	5.5
		1055.9	0.36	3.2			1058.8	0.23	13.5
		1066.8	0.20	3.2			1064.3	0.17	
$LiLuF_4$	π	1035.5	0.17	2.8	$Y_3Al_5O_{12}$		1014.9	0.22	2.3
		1054.3	0.24	3.0			1031.0	0.48	1.5
		1070.0	0.17	3.6	$YAlO_3$	***E*** ∥ ***a***	1044.2	1.55	2.7
	σ	1039.2	0.64	2.4			1055.6	0.71	3.6
		1048.8	0.34	4.9			1064.8	0.37	6.1
		1053.7	0.34	3.7		***E*** ∥ ***b***	1055.1	0.50	4.0
		1065.9	0.20	3.6			1066.4	0.13	8.0
						E ∥ ***c***	1055.5	0.22	4.0

[a] λ_{ESA} - peak wavelength; σ_{ESA} – peak ESA cross-section; $\Delta\lambda_{ESA}$ - absorption bandwidth (full width at half maximum, FWHM).

4. Energy-transfer upconversion

The ESA spectra in the IR spectral range can be also used for evaluating the concentration-independent parameter of one of the energy-transfer upconversion (ETU) processes for Tm^{3+} ions, i.e., $^3F_4 + {}^3F_4 \rightarrow {}^3H_4 + {}^3H_6$. This process acts against the cross-relaxation, $^3H_4 + {}^3H_6 \rightarrow {}^3F_4 + {}^3F_4$, refilling the higher-lying $^3H_4$ excited-state and depopulating the metastable $^3F_4$ state. It can significantly affect the performance of Tm lasers. In particular, it is detrimental for Tm lasers operating on the $^3F_4 \rightarrow {}^3H_6$ transition (at ~1.9 μm) [41]: strong ETU in highly Tm^{3+}-doped crystals is responsible for the increased laser threshold and additional heat generation possibly leading to higher risk of thermal fracture. In opposite, this ETU process could be useful for Tm lasers operating on the $^3H_4 \rightarrow {}^3H_5$ transition (at ~2.3 μm) as it refills the upper laser level at the expense of the metastable intermediate $^3F_4$ state [42]. In this way, pump quantum efficiencies up to 2 could be reached leading to laser slope efficiencies exceeding the Stokes limit. Thus, knowledge of the ETU parameter is of practical importance. Below, we describe the general calculation procedure and apply it to the particular case of Tm:$LiYF_4$.

The ETU rate was evaluated using the hopping (Burshtein) model describing a migration-assisted energy transfer [9]. This model treats the transfer of energy between donors as a random process until the excitation is transferred to an acceptor ion. First, two microparameters C_{DD} and C_{DA} were calculated from the overlap integrals between the SE and absorption (GSA or ESA) cross-section spectra [43]:

$$C_{DD} = \frac{3c}{8\pi^4 n^2} \int \sigma_{SE}(\lambda)\sigma_{GSA}(\lambda)d\lambda, \tag{4a}$$

$$C_{DA} = \frac{3c}{8\pi^4 n^2} \int \sigma_{ESA}(\lambda)\sigma_{SE}(\lambda)d\lambda, \tag{4b}$$

where D and A indicate a donor and an acceptor, respectively, C_{DD} represents a donor-donor process (energy migration) and C_{DA} – a donor-acceptor process (direct energy transfer), Fig. 10, c the speed of light in vacuum, n the mean refractive index of the host, σ_{SE} corresponds to the $^3F_4 \rightarrow {}^3H_6$ transition, σ_{GSA} and σ_{ESA} – to the transitions $^3H_6 \rightarrow {}^3F_4$ (GSA) and $^3F_4 \rightarrow {}^3H_4$ (ESA), respectively, λ is the light wavelength. For an anisotropic crystal, the transition cross-sections

should be polarization averaged. E.g., for Tm:$LiYF_4$, this means $\langle\sigma\rangle = (2\sigma_\sigma + \sigma_\pi)/3$, where the subscripts σ and π indicate the polarizations. In our case, the use of the hopping model is validated because $C_{DD} >> C_{DA}$ (i.e., the migration process among Tm^{3+} ions is more likely than direct energy transfer). Indeed, for Tm:$LiYF_4$, $C_{DD} = 3.26\times10^{-39}$ cm^6s^{-1} and $C_{DA} = 0.50\times10^{-43}$ cm^6s^{-1}.

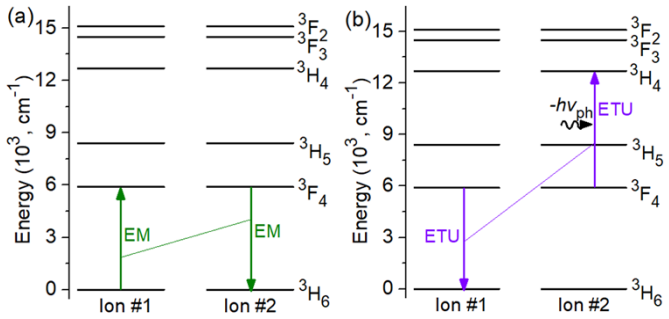

Fig. 10. Energy-transfer upconversion (ETU), $^3F_4 + {}^3F_4 \rightarrow {}^3H_4 + {}^3H_6$, for Tm^{3+} ions. Two elementary processes are shown: (a) energy-migration and (b) phonon-assisted "direct" ETU.

The macroscopic ETU rate in (s^{-1}) was then determined as [44]:

$$W_{ETU} = \pi\left(\frac{2\pi}{3}\right)^{5/2}\sqrt{C_{DD}C_{DA}}N_{Tm}^2, \tag{5}$$

where N_{Tm} is the doping concentration. There exist several ways to express the dependence of the ETU rate on N_{Tm} [23]:

$$W_{ETU} = K_{ETU}N_{Tm} = C_{ETU}N_{Tm}^2, \tag{6}$$

where K_{ETU} and C_{ETU} are the concentration-dependent and concentration-independent ETU parameters expressed in (cm^3s^{-1}) and (cm^6s^{-1}), respectively. When the migration process is very fast because of a high donor concentration, the K_{ETU} parameter is expected to be independent on the doping level (K_{ETU} = const). However, for most gain materials, the donor concentration typically stays below 20 at.% and the K_{ETU} parameter is proportional to the donor concentration, as expressed by Eq. (6). This situation is called migration-limited energy transfer [9].

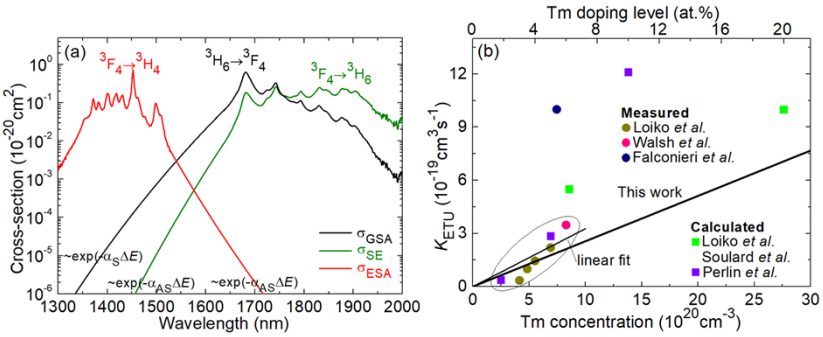

Fig. 11. Evaluation of the ETU parameter for Tm:$LiYF_4$: (a) polarization-averaged SE ($^3F_4 \rightarrow {}^3H_6$), GSA ($^3H_6 \rightarrow {}^3F_4$) and ESA ($^3F_4 \rightarrow {}^3H_4$) spectra plotted in semi-log scale, *solid curves* – measured spectra with phonon sidebands calculated using Eq. (7); (b) summary of the ETU parameters K_{ETU} reported so far: *symbols* – literature data, *line* – this work, calculation using Eqs. (4)-(6).

The considered ETU process is non-resonant and is phonon-assisted. The calculation of the overlap integrals between the SE and absorption (GSA and ESA) spectra should account for the multiphonon sidebands. The shape of the latter can be expressed as [45,46]:

$$\sigma_S = \sigma_0 \exp(-\alpha_S \Delta E), \tag{7a}$$

$$\sigma_{AS} = \sigma_0 \exp(-\alpha_{AS} \Delta E), \tag{7b}$$

where S and AS indicate Stokes and anti-Stokes process, respectively, ΔE is the energy mismatch between the vibronic (phonon-assisted) and the purely electronic transition, σ_0 is the cross-section at the photon energy of an electronic transition and the constants α_S and α_{AS} are determined by vibronic properties of the host material. For Tm:$LiYF_4$, we determined them in the present work to be $\alpha_S = 7.9\pm1\times10^{-3}$ cm^{-1} and $\alpha_{AS} = 12.1\pm2\times10^{-3}$ cm^{-1}.

Using Eqs. (4)-(6) and the spectroscopic data for Tm:$LiYF_4$, as shown in Fig. 11(a), we calculated the concentration-independent ETU parameter, $C_{ETU} = 2.56\times10^{-40}$ cm^{6}s^{-1}. In the previous studies, the ETU parameter (K_{ETU}) was typically reported for given Tm^{3+} doping concentrations, Fig. 11(b). In this work, the result of our calculation can be expressed as a linear dependence of K_{ETU} on N_{Tm} with a slope equal to C_{ETU}. Let us briefly review the methods used in previous studies to obtain the K_{ETU} values. So far, they were obtained from (i) luminescence-decay measurements [47,48], (ii) stationary luminescence-intensity measurements [42], (iii) theoretical calculations [49], and (iv) modeling of Tm laser performance [50,51]. Our results are in good agreement with the previously reported data, especially with the experimental ones from [42].

The determined C_{ETU} value should be compared with that for the cross-relaxation process, i.e., $C_{CR} = 0.25\pm0.03\times10^{-37}$ s^{-1}cm^6 for Tm:$LiYF_4$ [42]. One can see that the considered ETU process is by two orders of magnitude weaker that the CR one (for each particular Tm^{3+} doping level).

5. Conclusion

To conclude, we have studied excited-state absorption of Tm^{3+} ions in the near-infrared spectral range for a series of fluoride and oxide laser crystals using a dedicated pump-probe method. The considered ESA transitions originate from the metastable $^3F_4$ Tm^{3+} state and terminate at the higher lying $^3F_{2,3}$ and $^3H_4$ levels. The $^3F_4 \rightarrow {}^3F_{2,3}$ ESA channel is particularly attractive for upconversion pumping of Tm lasers via a photon avalanche mechanism. This pumping scheme can be used for obtaining laser emission at ~2.3 μm corresponding to the $^3H_4 \rightarrow {}^3H_5$ transition with commercial, power scalable and wavelength tunable Yb fiber lasers emitting slightly above 1 μm. The ESA line positions, cross-sections and spectral linewidths which are required for the design of upconversion pumped Tm lasers were measured in detail. Among the studied crystals, Tm:KY_3F_{10}, Tm:LiY/LuF_4 and Tm:$YAlO_3$ are identified as promising candidates for upconversion pumping. Regarding the second studied ESA channel, $^3F_4 \rightarrow {}^3H_4$, we show a route for calculating another key spectroscopic parameter for the development of Tm lasers, namely, the energy-transfer upconversion parameter. The ETU parameters are calculated from the absorption and emission overlap integrals using the hopping model.

Funding. Agence Nationale de la Recherche (ANR-19-CE08-0028, SPLENDID2)

Disclosures. The authors declare no conflicts of interest.

Data Availability. Data underlying the results presented in this paper are not publicly available at this time but may be obtained from the authors upon reasonable request.

References

1. J. Koetke, and G. Huber, "Infrared excited-state absorption and stimulated-emission cross sections of Er^{3+}-doped crystals," Appl. Phys. B **61**(2), 151-158 (1995).
2. N. V. Kuleshov, V. G. Shcherbitsky, V. P. Mikhailov, S. Kück, J. Koetke, K. Petermann, and G. Huber, "Spectroscopy and excited-state absorption of Ni^{2+}-doped $MgAl_2O_4$," J. Lumin. **71**(4), 265-268 (1997).
3. K. V. Yumashev, I. A., Denisov, N. N. Posnov, N. V. Kuleshov, and R. Moncorge, "Excited state absorption and passive Q-switch performance of Co^{2+} doped oxide crystals," J. Alloys Compd. **341**(1-2), 366-370 (2002).
4. Z. Burshtein, P. Blau, Y. Kalisky, Y. Shimony, and M. R. Kikta, "Excited-state absorption studies of Cr^{4+} ions in several garnet host crystals," IEEE J. Quantum Eletron. **34**(2), 292-299 (1998).

5. N. Garnier, R. Moncorgé, H. Manaa, E. Descroix, P. Laporte, and Y. Guyot, "Excited-state absorption of Tm^{3+}-doped single crystals at photon-avalanche wavelengths," J. Appl. Phys. **79**(8), 4323-4329 (1996).
6. S. Kück, L. Fornasiero, E. Mix, and G. Huber, "Excited state absorption and stimulated emission of Nd^{3+} in crystals. Part I: $Y_3Al_5O_{12}$, $YAlO_3$, and Y_2O_3," Appl. Phys. B **67**(2), 151-156 (1998).
7. C. Labbe, J. L. Doualan, S. Girard, R. Moncorgé, and M. Thuau, "Absolute excited state absorption cross section measurements in Er^{3+}:$LiYF_4$ for laser applications around 2.8 μm and 551 nm," J. Phys. Cond. Matter **12**(30), 6943 (2000).
8. S. D. Jackson, "Cross relaxation and energy transfer upconversion processes relevant to the functioning of 2 μm Tm^{3+}-doped silica fibre lasers," Opt. Commun. **230**(1-3), 197-203 (2004).
9. A. I. Burshtein, "Hopping mechanism of energy transfer," Sov. JETP Phys. **35**, 882–885 (1972).
10. L. Agazzi, K. Worhoff, and M. Pollnau, "Energy-transfer-upconversion models, their applicability and breakdown in the presence of spectroscopically distinct ion classes: A case study in amorphous Al_2O_3:Er^{3+}," J. Phys. Chem. C **117**(13), 6759-6776 (2013).
11. S. A. Pollack, D. B. Chang, and N. L. Moise, "Upconversion-pumped infrared erbium laser," J. Appl. Phys. **60**(12), 4077-4086 (1986).
12. T. Komukai, T. Yamamoto, T. Sugawa, and Y. Miyajima, "Upconversion pumped thulium-doped fluoride fiber amplifier and laser operating at 1.47 μm," IEEE J. Quantum Electron. **31**(11), 1880-1889 (1995).
13. F. Heine, E. Heumann, T. Danger, T. Schweizer, G. Huber, and B. Chai, "Green upconversion continuous wave Er^{3+}:$LiYF_4$ laser at room temperature," Appl. Phys. Lett. **65**(4), 383-384 (1994).
14. T. Hebert, R. Wannemacher, R.M. Macfarlane, and W. Lenth, "Blue continuously pumped upconversion lasing in Tm:$YLiF_4$," Appl. Phys. Lett. **60**(21), 2592-2594 (1992).
15. H. Scheife, G. Huber, E. Heumann, S. Bär, and E. Osiac, "Advances in up-conversion lasers based on Er^{3+} and Pr^{3+}," Opt. Mat. **26**(4), 365-374 (2004).
16. M. F. Joubert, S. Guy, B. Jacquier, and C. Linares, "The photon-avalanche effect: review, model and application," Opt. Mat. **4**(1), 43-49 (1994).
17. J. S. Chivian, W. E. Case, and D. D. Eden, "The photon avalanche: A new phenomenon in Pr^{3+}-based infrared quantum counters", Appl. Phys. Lett. **35**(2), 124-125 (1979).
18. M.E. Koch, A.W. Kueny, and W. E. Case, "Photon avalanche upconversion laser at 644 nm," Appl. Phys. Lett. **56**(12), 1083-1085 (1990).
19. W. Lenth, and R.M. Macfarlane, "Excitation mechanisms for upconversion lasers," J. Lumin. **45**(1-6), 346-350 (1990).
20. L. Guillemot, P. Loiko, R. Soulard, A. Braud, J.L. Doualan, A. Hideur, R. Moncorgé, and P. Camy, "Thulium laser at∼ 2.3 μm based on upconversion pumping," Opt. Lett. **44**(16), 4071–4074 (2019).
21. R. C. Stoneman, and L. Esterowitz, "Efficient, broadly tunable, laser-pumped Tm:YAG and Tm:YSGG CW lasers," Opt. Lett. **15**(9), 486-488 (1990).
22. J.F. Pinto, L. Esterowitz, and G.H. Rosenblatt "Tm^{3+}:YLF laser continuously tunable between 2.20 and 2.46μm," Opt. Lett. **19**(12), 883-885 (1994).
23. P. Loiko, and M. Pollnau, "Stochastic model of energy-transfer processes among rare-earth ions. Example of Al_2O_3: Tm^{3+}," J. Phys. Chem. C **120**(46), 26480-26489 (2016).
24. K. van Dalfsen, S. Aravazhi, C. Grivas, S. M. García-Blanco, and M. Pollnau, "Thulium channel waveguide laser with 1.6 W of output power and ∼80% slope efficiency," Opt. Lett. **39**(15), 4380-4383 (2014)
25. A. Tyazhev, F. Starecki, S. Cozic, P. Loiko, L. Guillemot, A. Braud, F. Joulain, M. Tang, T. Godin, A. Hideur and P. Camy, "Watt-level efficient 2.3 μm thulium fluoride fiber laser," Opt. Lett. **45**(20), 5788-5791 (2020).
26. J. Y. Allain, M. Monerie, and H. Poignant, "Blue upconversion fluorozirconate fibre laser," Electron. Lett. **26**(3), 166-168 (1990).
27. S. G. Grubb, K. W. Bennett, R. S. Cannon, and W. F. Humer, "CW room-temperature blue upconversion fibre laser," Electron. Lett. **28**(13), 1243-1244 (1992).
28. G. Qin, S. Huang, Y. Feng, A. Shirakawa, M. Musha, and K. I. Ueda, 2006. "Power scaling of Tm^{3+} doped ZBLAN blue upconversion fiber lasers: modeling and experiments," Appl. Phys. B **82**(1), 65-70 (2006).
29. J. W. Szela, and J. I. Mackenzie, "Excited-state absorption measurements of Tm^{3+}-doped crystals," Proc. SPIE **8433**, 84331O (2012).
30. J. Koetke, T. Jensen, and G. Huber, "Infrared stimulated emission and excited state absorption cross sections of Er^{3+}:YAG and Tm^{3+}:YAG lasers," in *Advanced Solid State Lasers*, B. Chai and S. Payne, eds., Vol. 24 of OSA Proceedings Series (Optica Publishing Group, 1995), paper IL5.
31. A. Braud, S. Girard, J. L. Doualan, M. Thuau, R. Moncorgé, A.M. Tkachuk, "Energy-transfer processes in Yb:Tm-doped KY_3F_{10}, $LiYF_4$, and BaY_2F_8 single crystals for laser operation at 1.5 and 2.3 μm," Phys. Rev. B **61**(8), 5280 (2020).
32. P. Le Boulanger, J. L. Doualan, S. Girard, J. Margerie, and R. Moncorgé, "Excited-state absorption spectroscopy of Er^{3+}-doped $Y_3Al_5O_{12}$, YVO_4, and phosphate glass," Phys. Rev. B **60**(16), 11380 (1999).
33. P. Loiko, J. L. Doualan, L. Guillemot, R. Moncorgé, F. Starecki, A. Benayad, E. Dunina, A. Kornienko, L. Fomicheva, A. Braud, and P. Camy, "Emission properties of Tm^{3+}-doped CaF_2, KY_3F_{10}, $LiYF_4$, $LiLuF_4$ and BaY_2F_8 crystals at 1.5 μm and 2.3 μm," J. Lumin. **225**, 117279 (2020).
34. L. Guillemot, P. Loiko, A. Braud, J.L. Doualan, A. Hideur, M. Koselja, R. Moncorge, and P. Camy, "Continuous-wave Tm:$YAlO_3$ laser at ∼2.3 μm," Opt. Lett. **44**(20), 5077-5080 (2019).

35. S. A. Payne, L. L. Chase, L. K. Smith, W. L. Kway, and W. F. Krupke, "Infrared cross-section measurements for crystals doped with Er^{3+}, Tm^{3+}, and Ho^{3+}," IEEE J. Quantum Electron. **28**(11), 2619–2630 (1992).
36. M. Dulick, G. E. Faulkner, N. J. Cockroft, and D. C. Nguyen, "Spectroscopy and dynamics of upconversion in Tm^{3+}:$YLiF_4$," J. Lumin. **48**, 517-521 (1991).
37. A. Lupei, V. Lupei, S. Grecu, C. Tiseanu, and G. Boulon, "Crystal-field levels of Tm^{3+} in gadolinium gallium garnet," J. Appl. Phys. **75**(9), 4652-4657 (1994).
38. A. Braud, "Caractéristiques spectroscopiques et émission laser de l'ion Tm^{3+} à 1.5 µm dans les fluorures," PhD dissertation (Université de Caen, 1999).
39. S. Renard, P. Camy, A. Braud, J.L. Doualan, and R. Moncorgé, "CaF_2 doped with Tm^{3+}: A cluster model," J. Alloys Compd **451**(1-2), 71-73 (2008).
40. L. Guillemot, P. Loiko, R. Soulard, A. Braud, J.L. Doualan, A. Hideur, and P. Camy, "Close look on cubic Tm:KY_3F_{10} crystal for highly efficient lasing on the $^3H_4 \rightarrow {}^3H_5$ transition," Opt. Express **28**(3) 3451–3463 (2020).
41. S. So, J.L. Mackenzie, D.P. Shepherd, W.A. Clarkson, J.G. Betterton, E.K. Gorton, "A power-scaling strategy for longitudinally diode-pumped Tm:YLF lasers," App. Phys. B, **84**(3), 389-393 (2006).
42. P. Loiko, R. Soulard, L. Guillemot, G. Brasse, J.L. Doualan, A. Braud, A. Tyazhev, A. Hideur, F. Druon, and P. Camy, "Efficient Tm:$LiYF_4$ lasers at 2.3 µm: Effect of energy-transfer upconversion," IEEE J. Quantum Electron. **55**(6), 1700212-1-12 (2019).
43. S. A. Payne, L. K. Smith, W. L. Kway, J. B. Tassano, and W. F. Krupke, "The mechanism of Tm to Ho energy transfer in $LiYF_4$," J. Phys.: Condens. Matter **4**(44), 8525-8542 (1992).
44. S. A. Payne, G. D. Wilke, L. K. Smith, and W. F. Krupke, "Auger upconversion losses in Nd-doped laser glasses," Opt. Commun. **111**(3-4), 263-268 (1994).
45. F. Auzel, "Multiphonon-assisted anti-Stokes and Stokes fluorescence of triply ionized rare-earth ions," Phys. Rev. B **13**(7), 2809–2817 (1976).
46. P. Loiko, E. Kifle, L. Guillemot, J.L. Doualan, F. Starecki, A. Braud, M. Aguiló, F. Díaz, V. Petrov, X. Mateos, and P. Camy, "Highly efficient 2.3 µm thulium lasers based on a high-phonon-energy crystal: evidence of vibronic-assisted emissions," J. Opt. Soc. Am. B **38**(2), 482-495 (2021).
47. M. Falconieri, A. Lanzi, G. Salvetti, and A. Toncelli, "Fluorescence dynamics in Tm,Ho:YLF following 800 nm pulsed laser excitation", App. Phys. B **66**(2), 153-162 (1998).
48. B. M. Walsh, N. P. Barnes, M. Petros, J. Yu, and U. N. Singh, "Spectroscopy and modeling of solid state lanthanide lasers: Application to trivalent Tm^{3+} and Ho^{3+} in $YLiF_4$ and $LuLiF_4$," J. Appl. Phys. **95**(7), 3255-3271 (2004).
49. E. Y. Perlin, A. M. Tkachuk, M. J. Joubert, and R. Moncorge, "Cascade-avalanche up-conversion in Tm^{3+}:YLF crystals," Opt. Spectrosc. **90**(5), 691-700 (2001).
50. P. Loiko, R. Soulard, G. Brasse, J.L. Doualan, B. Guichardaz, A. Braud, A. Tyazhev, A. Hideur, and P. Camy "Watt-level Tm:$LiYF_4$ channel waveguide laser produced by diamond saw dicing," Opt. Express **26**(19), 24653-24662 (2018).
51. R. Soulard, M. Salhi, G. Brasse, P. Loiko, J.L. Doualan, L. Guillemot, A. Braud, A. Tyazhev, A. Hideur, and P. Camy, "Laser operation of highly-doped Tm:$LiYF_4$ epitaxies: towards thin-disk lasers," Opt. Express **27**(6), 9287-9301 (2019).